Chemical Engineering Journal 496 (2024) 154027

Contents lists available at ScienceDirect

Chemical Engineering Journal

journal homepage: www.elsevier.com/locate/cej

Printed strips coated with a reticular organic framework for Non-Enzymatic detection of pesticides in the urine of rural workers

Thiago S. Martins [a,b,*], Fábio J.F.S. Henrique [c], Willian G. Birolli [d], José L. Bott-Neto [a], Henrique C.S. Silveira [d], Pierre M. Esteves [c], Osvaldo N. Oliveira Jr. [a]

[a] São Carlos Institute of Physics, University of São Paulo, 13560-970, São Carlos, SP, Brazil
[b] Imperial College London, Department of Chemistry, Molecular Sciences Research Hub, 82 Wood Lane, London W12 0BZ, United Kingdom
[c] Instituto de Química, Universidade Federal do Rio de Janeiro, 21941-909, Rio de Janeiro, RJ, Brazil
[d] Molecular Oncology Research Center, Barretos Cancer Hospital, Barretos, SP, Brazil

ARTICLE INFO

Keywords:
Covalent organic framework
Pesticides
Simultaneous detection
Urine
Non-invasive decentralized testing
Rural workers

ABSTRACT

Monitoring the exposure of rural workers to pesticides during spraying is essential to safeguard their health, and this should ideally be done on the farms. In this work, we developed sensor strips coated with a reticular covalent organic framework (COF) which can detect paraquat and carbendazim simultaneously in artificial and human urine. Using electrochemical methods, a selective detection can be made of paraquat and carbendazim across concentrations ranging from 0.05 to 10 μM, with detection limits of 0.01 and 0.05 μM, respectively. This performance and selectivity may be attributed to a combination of high surface area, chemical composition and pore size of the COF used. Tests with undiluted urine samples were positive for at least one pesticide for all the nine rural workers taking part in the study. This highlights the need for monitoring pesticide levels, that can be done with the sensors presented here as they may be used with portable instruments with no sample pre-treatment.

1. Introduction

Detection of pesticides in waters and in human body fluids is crucial to protect the environment and human health, especially of rural workers who are exposed directly while applying pesticides to the crop. Ideally, such monitoring should be done with technologies deployed on site, including in the farms, whose handling should be simple with portable, easy-to-operate instruments. This can be achieved using electrochemical sensors and biosensors. For the two pesticides of our interest here, namely paraquat and carbendazim, a number of reports exist. Paraquat was detected in pre-treated samples of malt and mint with an aptasensor comprising a three-dimensional nanocake-like Au-MXene structure and an Au pallet [1]. Electrodes coated with a two-dimensional FeCo-based bimetallic metal–organic framework were used to detect paraquat in pre-treated samples of apple, human serum, and fresh tea leaves [2]. A molecularly imprinted polymer-aptasensor based on hemin-Al-metal organic framework and gold nanoparticles was employed in detecting carbendazim in diluted samples of tap water, apple juice, and tomato juice [3]. Although these biosensors and sensors offered high sensitivity and specificity, their use could be limited owing to the need to incorporate biomolecules and require additional steps in sample preparation. These factors make it challenging to apply in complex matrices for self-testing and health monitoring.

An alternative is to employ optimized materials to obtain selective and high-performance sensors. Covalent organic frameworks (COFs) [4–6] are good candidates owing to their chemical stability, permanent porosity, and high specific surface area. Also, their structural diversity in virtue of the topological design of their building blocks has permitted applications in gas adsorption, storage, catalysis, sensing, and enzyme immobilization [7–15]. Particularly noteworthy is their potential in electrochemical sensing, since they may enhance selectivity, sensitivity, and diffusion speed by minimizing molecule clustering through ordered pore structures and adjustable functional groups [16–20]. Porosity allows for the free access of ions, facilitating contact with the electrodes, reducing the time required to reach reaction equilibrium and improving the repeatability of detection. Chemical composition may facilitate adsorption/desorption of the targeted substance on the COF surface. This process involves non-covalent interactions, including hydrogen

* Corresponding author at: São Carlos Institute of Physics, University of São Paulo, 13560-970 São Carlos, SP, Brazil; Imperial College London, Department of Chemistry, Molecular Sciences Research Hub, 82 Wood Lane, London W12 0BZ, United Kingdom.
E-mail address: thiagoserafimartins@gmail.com (T.S. Martins).

https://doi.org/10.1016/j.cej.2024.154027
Received 9 May 2024; Received in revised form 21 June 2024; Accepted 14 July 2024
Available online 15 July 2024

bonds, π–π interactions, hydrophobic interactions, and electrostatic interactions, which are relevant for the kinetics of electrochemical reactions.

In this paper, we report on printed strip sensors capable of non-invasive monitoring of paraquat and carbendazim in urine samples. The strip sensors are coated with a reticular organic framework, a COF referred to as RIO17 (Reticular Innovative Organic framework 17). The choice of paraquat and carbendazim was motivated by their importance for rural workers. Paraquat is a highly toxic, water-soluble herbicide which can cause multiple organ failure, particularly affecting the lungs, kidneys, and liver. Its acute exposure leads to significant pulmonary concentrations, resulting in alveolar damage and high mortality rates [21]. Furthermore, its use has been associated with an increased risk of Parkinson's disease among rural workers [22]. Carbendazim is a fungicide posing different but equally concerning risks. It can disrupt liver and kidney function, affect adipose tissues, interfere with blood cell production, and cause chromosomal abnormalities by inhibiting microtubule formation. This, in turn, affects nuclear division and generates DNA damage, raising concerns about its potential carcinogenic effects. [23]. Thus, this pesticide is considered a possible human carcinogen without safe exposure level [24]. As we shall show, with the sensor strips incorporating RIO17, one may implement on-site monitoring programs for rural workers, that today are not feasible with any existing technology.

2. Experimental details

2.1. Materials, reagents and solutions

The building block 1,3,5-triformylresorcinol (TFR), obtained according to ref. [25], was used to synthesize the COF referred to as RIO17, which also includes acetic acid (Rioquímica, Brazil), 1,4-dioxane (Isofar, Brazil), mesitylene (Sigma-Aldrich, USA), methanol (Isofar, Brazil), dimethylformamide (Merck, Germany), and tetrahydrofuran (Isofar, Brazil). Sodium sulfate (Na_2SO_4), sodium citrate dihydrate ($Na_3C_6H_5O_7{\cdot}2H_2O$), urea ($CH_4N_2O$), potassium chloride (KCl), sodium chloride (NaCl), calcium chloride dihydrate ($CaCl_2{\cdot}2H_2O$), ammonium chloride (NH_4Cl) sodium oxalate ($Na_2C_2O_4$), magnesium sulfate ($MgSO_4$), sodium dihydrogen phosphate (NaH_2PO_4), disodium hydrogen phosphate (Na_2HPO_4), paraquat, carbendazim, D-glucose, uric acid, lactic acid, amoxicillin, glyphosate, 2,4-dichlorophenoxyacetic acid (2,4-D), fipronil sulfone were obtained from Sigma-Aldrich (USA). Carbon conductive ink (LOCTITE, Eletrodag 423SS E&C, Germany) and silver paste (TICON, Code 90701, Brazil) were used to produce the screen-printed sensors on polyethylene terephthalate. The artificial urine was prepared using a modified procedure from Sarigul et al. [26], which involved dissolving: 170 mg Na_2SO_4, 72 mg $Na_3C_6H_5O_7{\cdot}2H_2O$, 1500 mg CH_4N_2O, 230.8 mg KCl, 175.6 mg NaCl, 18.5 mg $CaCl_2{\cdot}2H_2O$, 126.6 mg NH_4Cl, 3.5 mg $Na_2C_2O_4$, 108.2 mg $MgSO_4$, 291.2 mg NaH_2PO_4, and 83.1 mg Na_2HPO_4 in 1 L ultrapure water. This water was obtained from a Millipore system and exhibited a resistivity of 18.2 MΩ cm.

RIO17 was synthetized through a hydrothermal method using *p*-phenylenediamine and 1,3,5-triformylresorcinol as the building blocks. In a 48 mL heavy-wall pressure vessel reactor, 0.388 g TFR block (1 equivalent, 2 mmols), 0.324 g *p*-phenylenediamine (1.5 equivalents, 3 mmols), 13.6 mL 1,4-dioxane, 1.2 mL mesitylene, and 4.6 mL 6 M acetic acid were added. The reactor was then placed in a bath heated to 120 °C under agitation and maintained for 169 h. The resulting mixture was then filtered and washed successively with MeOH, DMF, and THF, yielding black crystals. The wet filter paper containing the crystals was separated and soaked in THF for 168 h. THF was replaced with absolute ethanol, and the mixture was transferred to the supercritical CO_2 SAMDRI-PVT-3D drying equipment (Tousimis). After the CO_2 treatment, the dried crystals were weighed, resulting in 0.68 g of RIO17.

2.2. Techniques for Characterization

The transmission electron microscopy (TEM) images on lacey carbon grid (200 mesh/cooper) were recorded on a TECNAI G 20 microscope. Field emission gun scanning electron microscopy (FEG-SEM) images were taken in a Zeiss Sigma (Germany). Images of pure COF were obtained on a silicon substrate. Textural properties were assessed through nitrogen physisorption conducted at − 196 °C using a Nova 2200e apparatus, pre-treated in the FLOVAC Degasser equipment, Quantachrome. Thermogravimetric analysis (TGA) and derivative thermogravimetry (DTG) were performed using a TG 209 F1 Iris instrument, Netzsch. The measurement was conducted in a nitrogen (N_2) atmosphere using a heating ramp of 10 °C per minute. X-ray diffraction analysis (XRD) was performed with a Rigaku X-ray diffractometer. Fourier transform infrared spectroscopy analysis (FTIR) was carried on an FTLA-2000 spectrometer over the spectral range of 400 – 4000 cm^{-1} with samples prepared as diluted KBr pellets. Cross-polarization magic angle spinning carbon-13 nuclear magnetic resonance (CPMAS ^{13}C NMR) spectra were collected on a 9.4 T WB Bruker Avance III spectrometer. The electrochemical measurements and electrochemical impedance spectroscopy (EIS) were performed in 100 μL solutions using an Autolab potentiostat, PGSTAT30 model, controlled with NOVA 2.1.4 software. EIS experiments were carried out in 0.1 M KCl with 5 mM of ferrocyanide and 5 mM of ferricyanide, under an open circuit voltage within a frequency range from 100 kHz to 0.1 Hz and excitation amplitude of 10 mV. All the redox potentials were recorded versus silver/silver chloride (Ag/AgCl) ink printed on one of the carbon electrodes.

2.3. Preparation of the sensing strips

The sensor strips were manufactured on a flexible polyethylene terephthalate substrate using a low-cost and scalable screen-printing technique, as described by Martins et al. [27] and illustrated in Fig. 1**a**. Prior to modification, the strips underwent electrochemical treatment via cyclic voltammetry (CV) to eliminate nonconductive compounds and impurities from the carbon ink: two cycles were conducted from − 2.5 to 2.5 V at a rate of 100 mV s^{-1} in a 0.5 M H_2SO_4 solution [28]. Then, 6 μL RIO17 (1 mg mL^{-1} in water) was applied to the working electrode and dried under vacuum at room temperature.

2.4. Electrochemical measurements

Fig. 2**a** displays a photograph of the sensor setup, including a lab-made printed strip and its corresponding connector. The detection of carbendazim and paraquat in artificial urine or human urine samples was carried out without any pre-treatment or dilution steps. Except for the analyses with human urine, other studies were performed using artificial urine prepared as described in **Section 2.1** and containing known concentrations of carbendazim and paraquat, with concentrations ranging from 0.05 to 10 μM. A 100 μL sample was added to the sensing area, and the electrochemical response was obtained by square wave voltammetry (SWV) from − 1.1 to 0.95 V with a step potential of 3 mV pulse amplitude at 10 Hz. The limit of detection (LOD) was determined using LOD = 3 S_b/b, where S_b is the standard deviation of the blank and b is the slope of the analytical curve.

2.5. Sensing with human urine

To validate the sensor strips, urine samples from nine rural workers directly exposed to the pesticides carbendazim and paraquat were utilized. This study followed ethical regulations within the prospective cohort Rural Workers and Cancer: A Cohort Study (RUCAN study), in that a group was selected based on their involvement in carbendazim and paraquat spraying activity. All participants signed the Informed Consent Form which received approval from the Research Ethics

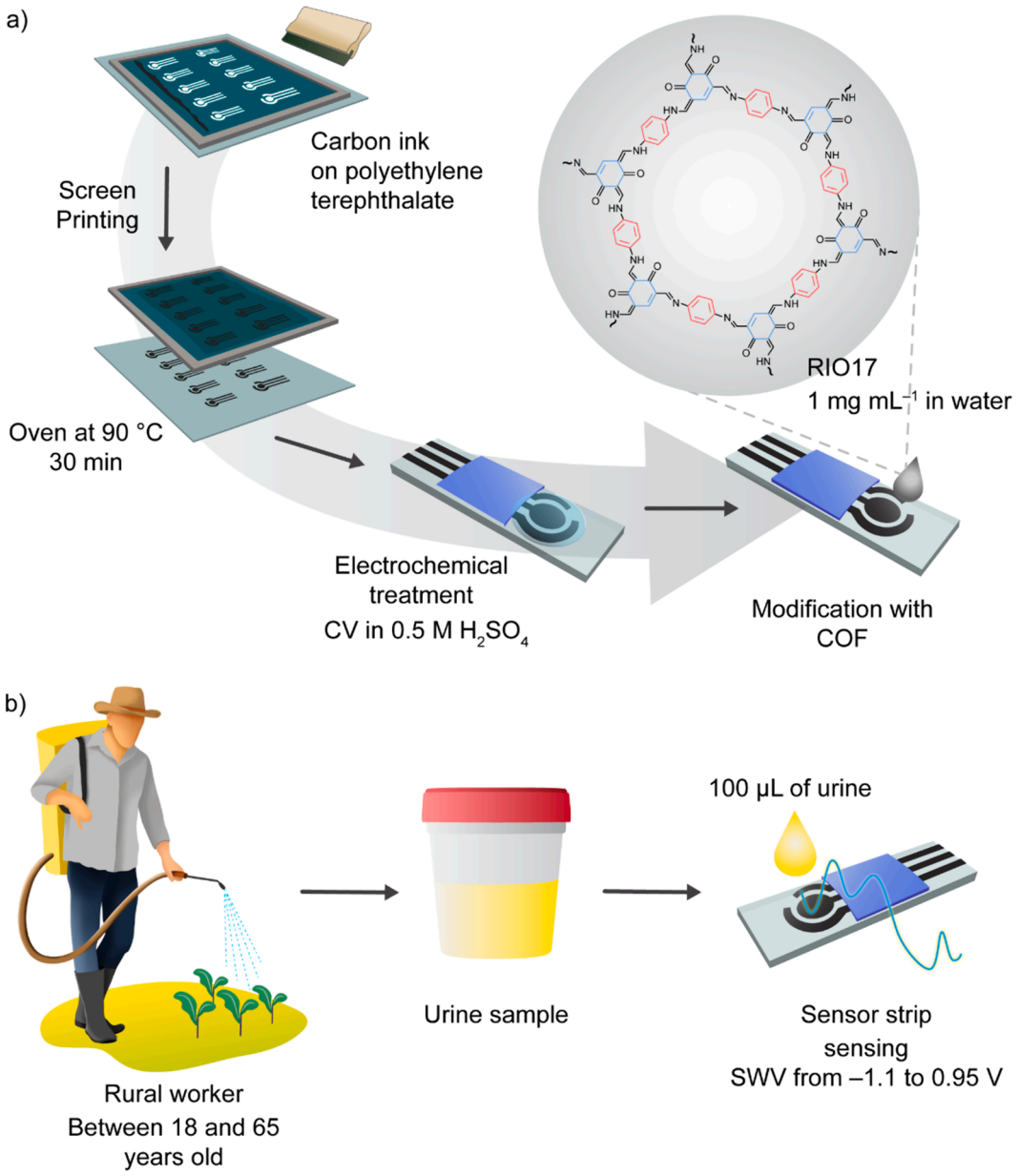

Fig. 1. Concept of printed sensor strips: (a) illustration of the preparation of printed strips for decentralized self-testing of pesticides in urine; (b) scheme for non-invasive simultaneous detection of paraquat and carbendazim in urine.

Committee of the Barretos Cancer Hospital, under protocol n°. 1585/2018. Male individuals aged between 18 and 65 years were recruited from 2021 to 2023 via an active search at agricultural communities of Barretos region (São Paulo, Brazil), using data from the Secretariat of Agriculture and Supply of the São Paulo State which identifies family farming. Participants answered a self-report questionnaire followed by sample collection [29]. First morning voids of urine were collected in specialized storage containers and maintained at 4 °C for no longer than 12 h. Samples were stored at − 80 °C at the biobank of the Barretos Cancer Hospital [30]. The concentrations of paraquat were obtained by interpolation on an analytical curve, using current values subtracted from the blank measured in artificial urine at pH 4.

3. Results and discussion

3.1. Characterization of RIO17

The morphology of RIO17 and the sensor was analyzed using FEG-SEM. Fig. 2**b-d** display particle aggregates forming a sponge-like structure with numerous interconnected cavities, or macropores, as discussed below. Fig. 2**e and 2f** present FEG-SEM images of the printed strip surface and its version modified with RIO17, respectively. In Fig. 2**e**, quasi-spherical carbon particles are seen on the printed strip, comprising carbon conductive ink. An increase in porosity of RIO17-modified electrode surface in Fig. 2**f**.

The TEM image in Fig. 3**a** shows nearly spherical aggregates of RIO17 whose average size is 137.7 ± 2.8 nm according to the histogram in Fig. 3**b**. The N_2 adsorption–desorption isotherms in Fig. 3**c** for RIO17 have a classical type I shape, indicating predominant microporosity. **Table S1** displays data regarding specific surface area (S_{BET}), micropore area ($S_{microporous}$), external or mesoporous area ($S_{mesoporous}$), and micropore volume for RIO17. The experimental values for S_{BET}, $S_{microporous}$, $S_{mesoporous}$, and micropore volume are 847 m^2/g, 806 m^2/g, 41 m^2/g and 0.302 cc g^{-1}, respectively. Fig. 3**d** depicts the thermogravimetric analysis of RIO17. The 20 % mass loss at 120 °C refers to solvents and moisture within the pores. RIO17 remained stable up to 360 °C.

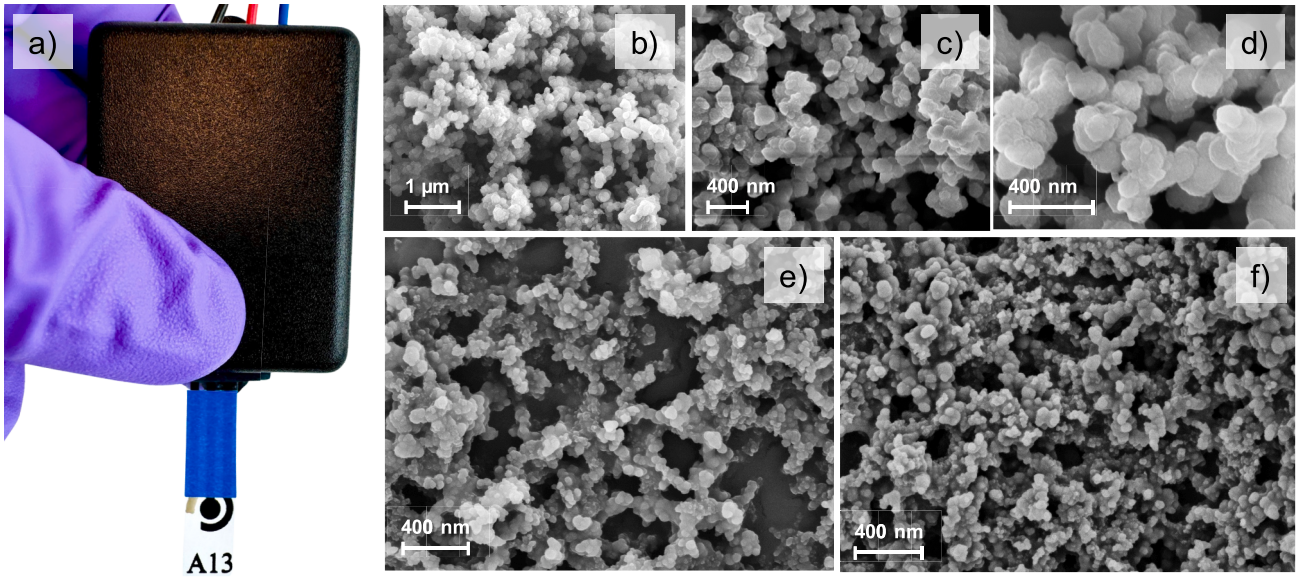

Fig. 2. a) photograph of the sensor setup, consisting of the lab-made printed strip and its corresponding connector. feg-sem images of rio17 on silicon substrate with magnifications of (b) 25 kx, (c) 50 kx, and (d) 100 kx. FEG-SEM images with 100 kx magnification of (e) the printed strip and (f) the printed strip modified with RIO17.

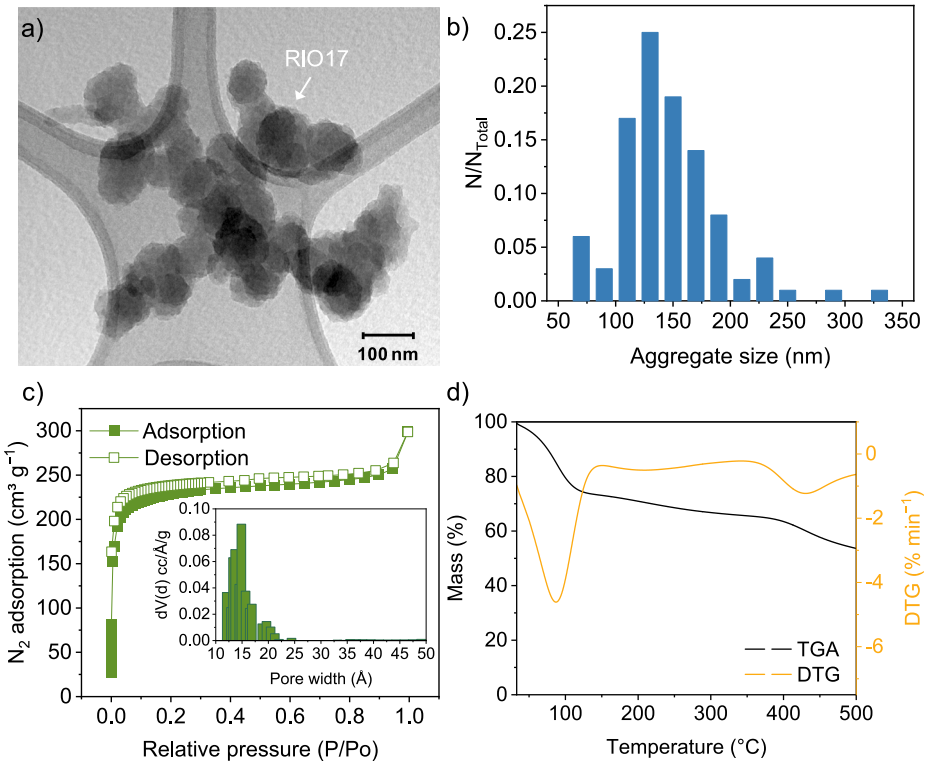

Fig. 3. Characterization of RIO17, consisting of: (a) TEM image; (b) size-distribution histogram for approximately 100 aggregates; (c) adsorption–desorption isotherms for N_2, with the pore size distribution in the inset; (d) TGA and DTG analysis.

Fig. 4**a** shows the theoretical diffractogram calculated by the Vesta program and the experimental one for RIO17. Diffractogram peaks appear at 2θ values of 4° and 5°, corresponding to the Miller index planes (1 0 0) associated with the growth of the structural 2D sheet. Peaks are also seen at 8° for plane (1 1 0), 12° for plane (2 1 0), and 27° for plane (0 0 1), with the latter attributed to structure stacking. The XRD results suggest RIO17 possesses a crystalline structure similar to that predicted by simulated XRD data. The FTIR spectrum for RIO17 in Fig. 4**b** has the band assigned to C=N stretching bonds at 1571 cm^{-1} and no band which could be related to aldehyde carbonyl (2875 cm^{-1}), thus indicating the absence of the precursor, 1,3,5-triformylresorcinol. The chemical structure of RIO17 was confirmed by solid-state CP-MAS ^{13}C NMR (Fig. 4**c-d**).

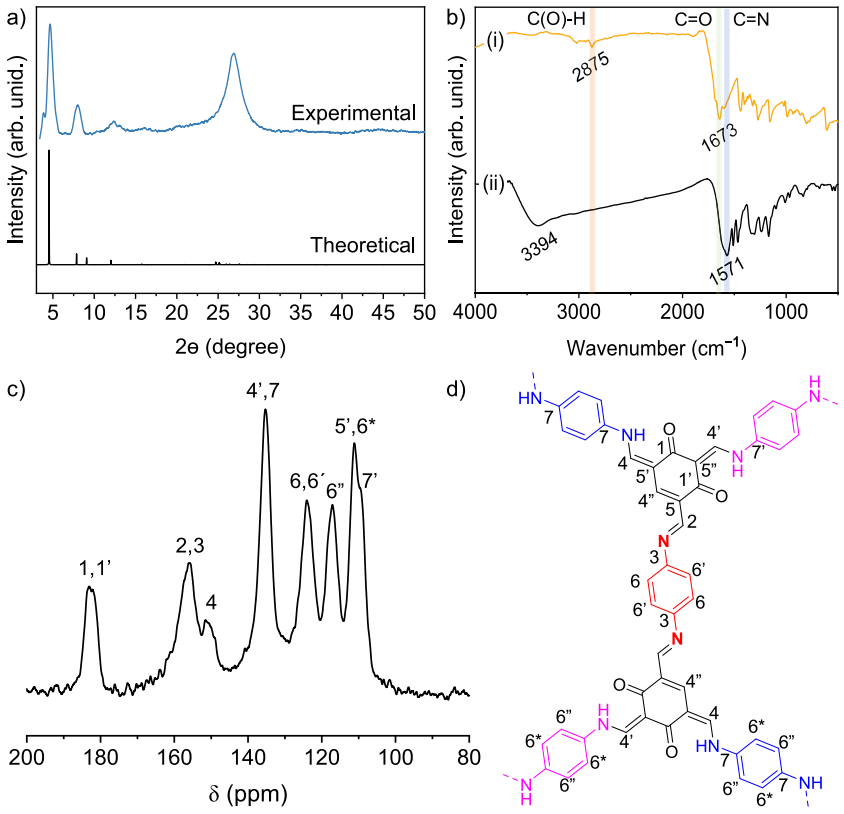

Fig. 4. (a) Experimental and theoretical XRD of RIO17. (b) FTIR analysis for (i) 1,3,5-triformylresorcinol and (ii) RIO17. (c) CP-MAS ^{13}C NMR and (d) a segment of the molecular structure of RIO17.

3.2. *Performance of sensor strips*

As shown in Fig. 1**b**, the detection of paraquat and carbendazim is based on a redox reaction during a potential scan as a small sample volume is dropped onto the sensor. Using SWV within a potential range from − 1.1 V to 0.95 V, these pesticides can be selectively detected in

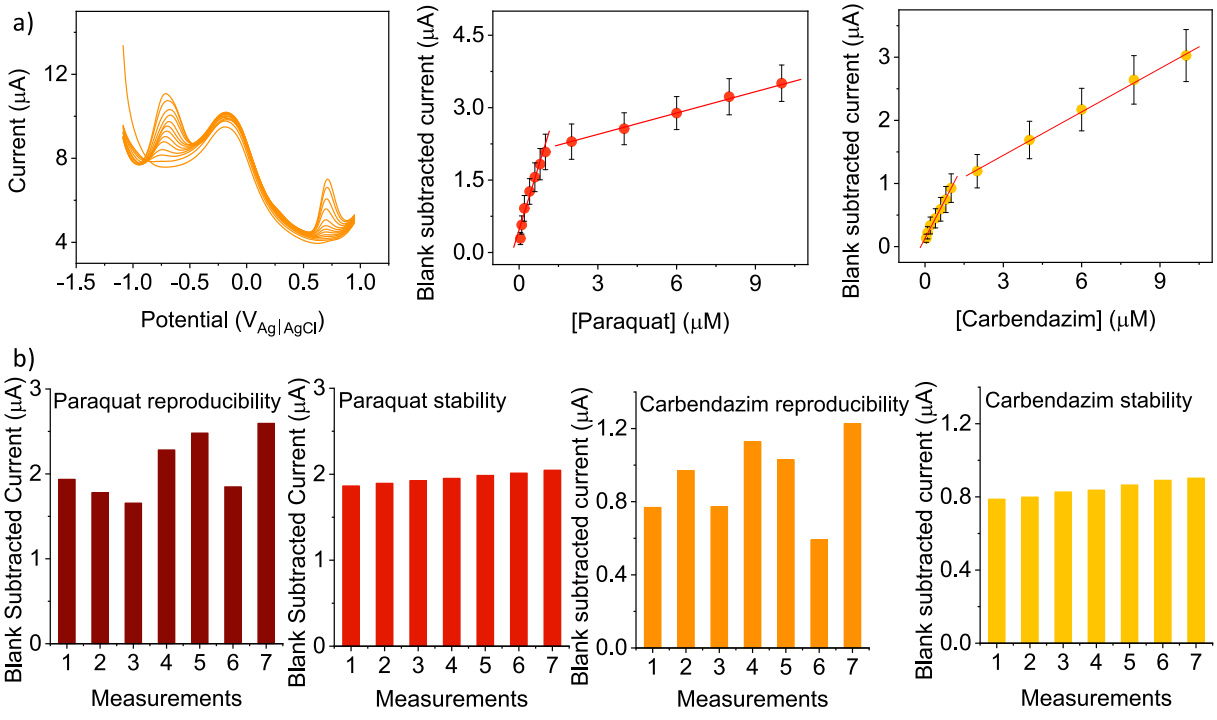

Fig. 5. (a) Analytical curves within the concentration range from 0.05 to 10 μM. The data are presented as the mean (n = 7), with error bars representing the standard deviation. (b) Reproducibility and stability tests in the presence of both paraquat and carbendazim at 1 μM. All measurements were conducted in artificial urine using SWV for the simultaneous detection of both pesticides within the potential range from − 1.1 to 0.95 V.

human urine, as will be shown later. **Figure S1a** in the Supporting Information indicates that RIO17 coating reduced the charge transfer resistance (R_{ct}) from 1.92 to 1.58 kΩ. This decrease in resistance indicates an improvement in electron transfer efficiency, likely due to the porosity and π-π conjugated structure of COF [31,32]. Also, as observed in the CV measurements in **Figure S1b**, the incorporation of RIO17 led to an increased in current with peaks at around − 0.7 and 0.8 V associated with the oxidation of paraquat and carbendazim, with an almost insignificant increase in the electrical double layer region. This enhancement contributes to the overall performance of the electrode.

Fig. 5**a** shows the SWV currents recorded in artificial urine increased linearly across two concentration ranges: from 0.05 to 1 μM and from 2 to 10 μM, for both paraquat and carbendazim. The linear relationships are described by the following equations: I (μA) = $4.17 \times 10^{-7} + 1.78 \times$ [Paraquat] (μM) ($R^2 = 0.960$, n = 7) and I (μA) = $1.97 \times 10^{-6} + 0.15 \times$ [Paraquat] (μM) ($R^2 = 0.998$, n = 7) for paraquat. For carbendazim, the equations are I (μA) = $1.33 \times 10^{-7} + 0.78 \times$ [Carbendazim] (μM) ($R^2 = 0.992$, n = 7) and I (μA) = $7.60 \times 10^{-7} + 0.23 \times$ [Carbendazim] (μM) ($R^2 = 0.998$, n = 7). [Paraquat] or [Carbendazim] is the pesticide concentration, and I is the blank-subtracted current. The LOD were estimated at 0.01 μM and 0.12 μM for paraquat and 0.02 μM and 0.05 μM for carbendazim. The sensing performance of the strips, particularly in terms of its limit of detection and linear range, is ideal for monitoring these pesticides according to the concentration intervals reported in the literature. It is worth emphasizing detection could be performed in less than 70 s using a sample volume of just 100 μL. Table 1 compares the performance of the disposable strips with the literature, which confirms they are competitive, being the only ones applied to urine for the two pesticides.

To evaluate the reproducibility and stability of the sensors, tests were carried out using SWV in artificial urine for simultaneous detection of 1 μM carbendazim and 1 μM paraquat. The results in Fig. 5**b** confirmed the reproducibility across seven different devices, with a relative standard deviation (RSD) of 17.7 % for paraquat and 24.3 % for carbendazim. Stability tests were conducted using the same strip to assess sensor behavior during the construction of the analytical curve. The sample volume was exchanged between each measurement, resulting in an RSD of 3.3 % for paraquat and 5.2 % for carbendazim.

Since the pH of human urine may fluctuate from acidic to basic [26], we investigated the impact of pH within a range of 4 to 8 on the electrochemical behavior of the sensors. A concentration of 1.0 μM of paraquat and carbendazim in artificial urine was used. **Figure S2** in the Supporting Information shows the peak potentials for carbendazim shifted to less positive values with increasing pH. In contrast, for paraquat the peak potentials remained relatively stable. A larger variation in current is observed only at urine pH 4, which could affect the measurement accuracy. This observation is particularly relevant given the average pH of human urine is around 6.0. The ability of these sensor strips to detect substances across the typical pH range of human urine confirms their potential for real-world applications.

The selectivity of the sensor was tested in artificial urine against substances commonly found in urine: glucose, uric acid, lactate, nitrate, nitrite, amoxicillin, fipronil sulfone, 2,4-D, and glyphosate. We first measured the sensor response to 1 μM paraquat and carbendazim. Then, we measured 1 μM of paraquat and carbendazim along with 1 mM or 5 μM of each interfering substance. Fig. 6 shows these substances had a minimal impact on the current for paraquat and carbendazim. The high selectivity of the flexible sensor against these interfering substances may be associated with a combined effect of pore size and functional groups in RIO17 and applied potential. These factors appear to have been essential for the adsorption/desorption required for detecting their oxidation processes. **Figure S3** supports the absence of significant mutual interference, indicating it is feasible to detect the two pesticides simultaneously with the same sensor.

The effectiveness of the sensor strip was evaluated using real urine samples from rural workers directly exposed to the pesticides in spraying activity. The procedure involved applying 100 μL of the samples onto the sensor without any treatment or dilution. **Figure S4** displays the SWV responses of the analyzed samples, while Table 2 provides an indication of a positive or negative response for the presence of paraquat and carbendazim. Urine samples of nine workers were analyzed, which had acidic pH and high levels of uric acid, probably due to dietary patterns of the individuals tested [47]. The low pH, combined with the high concentration of uric acid, caused distortions in the baseline of the measurements, making it difficult to quantify carbendazim at pH levels around 4, as previously observed in the pH study. Nevertheless, the sensor maintains its capability to detect carbendazim at pH levels around 4 (even without quantifying it). It can quantify carbendazim at pHs from 5 to 8 and paraquat within a pH range from 4 to 8. All nine rural workers tested positive for carbendazim, while 4 workers had paraquat concentrations ranging 0.26 to 0.75 μM. These results are indeed worrying because these pesticides in the body can pose health hazards [24,48]. They also highlight the need for monitoring workers' health with on-site analysis. The sensor strips reported here fulfil the

Table 1
Overview of electrochemical sensors to detect paraquat and carbendazim. *

Electrode	Potable	Analyte	Sample	Sample preparation or dilution steps	Detection range (μM)	LOD (μM)	Ref
N-rGO/Pd-LaV/GCE	No	Carbendazim	Food	Yes	0.015–10	0.002	[33]
NiCo-LDH/GCE	No	Carbendazim	Water	No	0.006–14.1	0.001	[34]
Au@Pt/CNHs@rGO/GCE	No	Carbendazim	Food	Yes	0.05–50	0.002	[35]
Yb_2O_3/f-CNF/GCE	No	Carbendazim	Food and water	Yes	0.05–155, 156–3035	0.006	[36]
Gpt-PLA	Yes	Carbendazim	Food	Yes	0.5–50	0.03	[37]
Ce-MOF@PANI/CC	No	Carbendazim	Food and water	Yes	0.1–80	0.01	[38]
TiO_2/rGO/CPE	No	Carbendazim	Soil and water	Yes	0.05–1000	0.008	[39]
RIO17/Printed Strip	Yes	Carbendazim	Urine	No	0.05–1, 2–10	0.02	This work
Ag-TiO_2/MXene/GCE	No	Paraquat	Food	Yes	0.05–1, 1–15	0.01	[40]
CA/SPCE	Yes	Paraquat	Food and water	No	0.1–1.0	0.02	[41]
B:CNWs	No	Paraquat	Water	No	0.1–1, 2–12	0.47	[42]
CoPc-cou-f-MWCNT/3-HT|Au	No	Paraquat	Water	No	0.584–1000	0.193	[43]
MnO_2@cellulose/SPCE	Yes	Paraquat	Water	No	2–200	1	[44]
CoS_2-GCN/GCE	No	Paraquat	Food	Yes	0.02–1, 1–13	0.004	[45]
P3ABA/GO-AuNPs/SPCE/	Yes	Paraquat	Water	Yes	0.001–100	0.0004	[46]
RIO17/Printed Strip	Yes	Paraquat	Urine	No	0.05–1, 2–10	0.01	This work

* GCE: glassy carbon electrode; N-rGO: N-doped reduced graphene oxide; Pd-LaV: Pd-doped lanthanum vanadate; CNHs: carbon nanohorns; Au@Pt:gold platinum core–shell nanoparticles; Yb_2O_3: ytterbium oxide nanorod; f-CNF: carbon nanofiber; Gpt: graphite; PLA: polylactic acid; CA: cellulose acetate; SPCE: screen printed carbon electrode; B:CNWs: boron-doped carbon nanowalls; CoPc-cou: coumarin tetra-substituted cobalt phthalocyanine; f-MWCNT: carboxylic acid functionalized multiwalled carbon nanotubes; 3-HT: poly(3-hexylthiophene); Au: gold sputtered electrode; MnO_2@cellulose: cellulose incorporated with manganese oxide; Ce-MOF: cerium metal–organic framework; PANI: polyaniline; CC: carbon cloth, CoS_2: cobalt disulfide, GCN: graphitic carbon nitride; P3ABA: poly(3-aminobenzoic acid); CPE: carbon paste electrode.

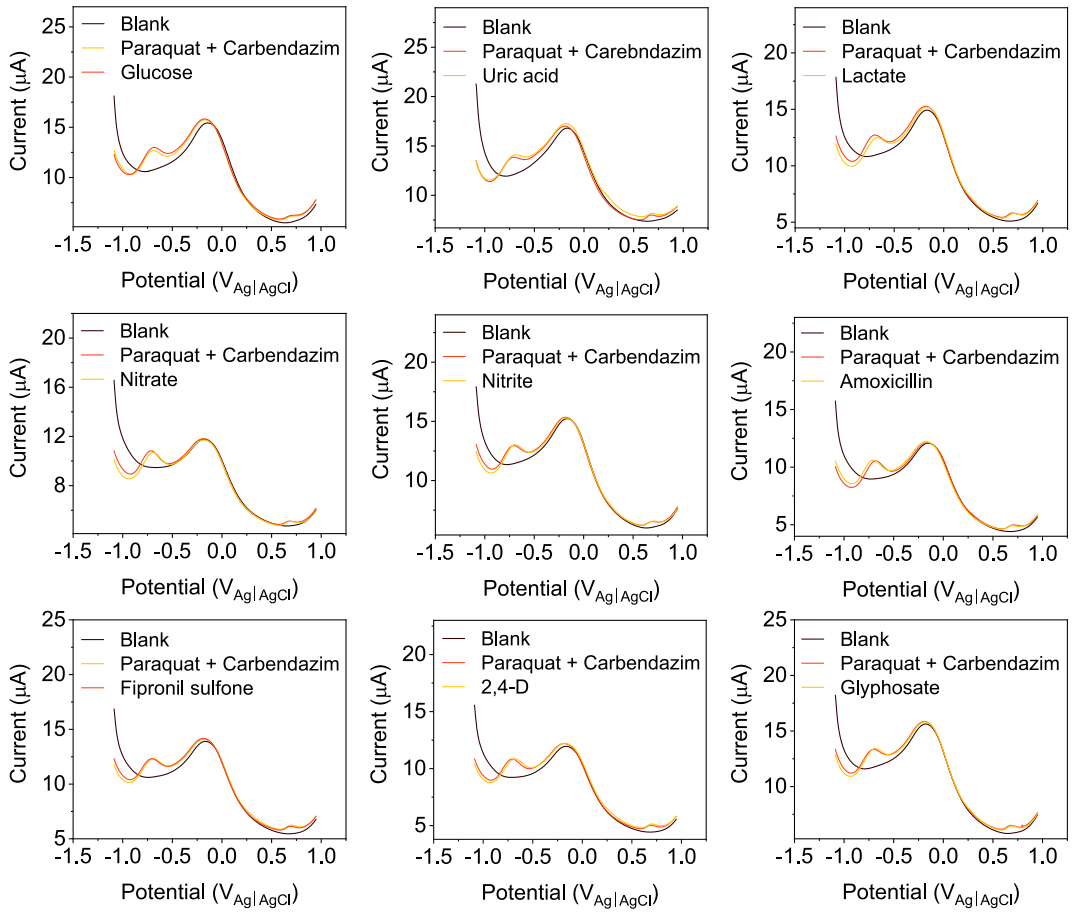

Fig. 6. Selectivity analysis in the presence of potential interfering molecules: voltammetric response of the sensor strips when exposed to potential interferent molecules commonly found in human urine samples, including glucose (1 mM), uric acid (5 μM), lactate (5 μM), nitrate (5 μM), nitrite (5 μM), amoxicillin (5 μM), fipronil sulfone (5 μM), 2,4-D (5 μM), and glyphosate (5 μM), while simultaneously detecting paraquat and carbendazim at 1 μM. The SWV measurements were performed in artificial urine over a potential range from − 1.1 V to 0.95 V.

Table 2
Results from detection of pesticides paraquat and carbendazim in the urine of rural workers. The concentration of paraquat could be quantified while for carbendazim it was only possible to determine its presence.

Patient	Paraquat contamination (μM)	Carbendazim contamination
1	No	Yes
2	0.52	Yes
3	0.75	Yes
4	0.64	Yes
5	No	Yes
6	0.26	Yes
7	No	Yes
8	No	Yes
9	No	Yes

stringent requirements for this type of analysis: they are lowcost, disposable, allowing for monitoring without sample preparation or dilution steps, with measurements which can be performed using portable instruments.

4. Conclusion

We developed sensor strips coated with COF RIO17 which could detect the pesticides paraquat and carbendazim in the urine of rural workers. This selective detection of the two pesticides, without interference from other substances in urine, was achieved in undiluted urine, without biomolecules which could function as recognition agents. The sensor strips were reproducible and sensitive in the linear ranges between 0.05 and 10 μM with limit of detections of 0.01 and 0.05 μM for paraquat and carbendazim. Detection could be carried out with small sample volumes, i.e. 100 μL, in less than 70 s. Such a performance may be attributed to a combination of surface area, pore size, and chemical composition of RIO17. Using these sensors is advantageous over standard analytical techniques by enabling rapid on-site detection of both pesticides simultaneously, without the need for additional sample preparation steps. It represents an advancement toward the trend of point-of-care testing technologies, providing rural workers with an accessible tool to monitor their exposure to agrochemicals and safeguard their health. That all rural workers were tested positive for at least one pesticide, this type of monitoring seems essential. Although we did not emphasize data analysis, our approach is ideal for collecting large volumes of data, which can subsequently be processed using statistical, computational, and even machine learning methodologies.

CRediT authorship contribution statement

Thiago S. Martins: Writing – review & editing, Writing – original draft, Visualization, Validation, Supervision, Resources, Project administration, Methodology, Investigation, Funding acquisition, Formal analysis, Data curation, Conceptualization. **Fábio J.F.S. Henrique:** Writing – review & editing, Methodology, Investigation, Formal analysis. **Willian G. Birolli:** Writing – review & editing, Resources, Methodology. **José L. Bott-Neto:** Writing – review & editing, Visualization, Resources, Funding acquisition, Formal analysis. **Henrique C.S.**

Silveira: Writing – review & editing, Resources, Methodology, Investigation, Funding acquisition. **Pierre M. Esteves:** Writing – review & editing, Resources, Formal analysis. **Osvaldo N. Oliveira Jr.:** Writing – review & editing, Supervision, Resources, Funding acquisition.

Declaration of competing interest

The authors declare that they have no known competing financial interests or personal relationships that could have appeared to influence the work reported in this paper.

Data availability

Data will be made available on request.

Acknowledgments

The authors are grateful for the financial support from CAPES, INEO, CNPq, FAPERJ, and FAPESP (2022/03758-0, 2022/15122-3, 2019/13514-9, 2022/00243-0, 2018/23105-6, and 2018/22214-6). Also, the Ministry of Health from Brazil, grant numbers 881187/2018, 879335/2018, 894586/2019, and 894588/2019. Henrique Silveira (grant 314247/2021-1) is recipient of CNPq productivity fellowship.

Appendix A. Supplementary data

Supplementary data to this article can be found online at https://doi.org/10.1016/j.cej.2024.154027.

References

[1] Q.-B. Xu, J. Wang, P.-Y. Song, Y. Li, N. Long, W.-J. Wu, L.-D. Zhou, L.-C. Shi, R.-L. Pan, W.-J. Kong, 3D nanocake-like Au-MXene/Au pallet structure–based label-free electrochemical aptasensor for paraquat determination, Microchim. Acta 191 (2024) 33, https://doi.org/10.1007/s00604-023-06111-4.
[2] H. Shu, T. Lai, S. Wang, M. Li, H. Li, T. Chen, X. Xiao, Y. Wang, The interaction between Fe and Co dual active sites for promoting ultra-sensitive detection of trace paraquat, Chem. Eng. J. 480 (2024) 148180, https://doi.org/10.1016/j.cej.2023.148180.
[3] H. Khosropour, M. Keramat, W. Laiwattanapaisal, A dual action electrochemical molecularly imprinted aptasensor for ultra-trace detection of carbendazim, Biosens. Bioelectron. 243 (2024) 115754, https://doi.org/10.1016/j.bios.2023.115754.
[4] P.J. Waller, F. Gándara, O.M. Yaghi, Chemistry of Covalent Organic Frameworks, Acc. Chem. Res. 48 (2015) 3053–3063, https://doi.org/10.1021/acs.accounts.5b00369.
[5] M.S. Lohse, T. Bein, Covalent Organic Frameworks: Structures, Synthesis, and Applications, Adv. Funct. Mater. 28 (2018), https://doi.org/10.1002/adfm.201705553.
[6] A.P. Côté, A.I. Benin, N.W. Ockwig, M. O'Keeffe, A.J. Matzger, O.M. Yaghi, Porous, Crystalline, Covalent Organic Frameworks, Science (1979) 310 (2005) 1166–1170. https://doi.org/10.1126/science.1120411.
[7] J. Gan, A.R. Bagheri, N. Aramesh, I. Gul, M. Franco, Y.Q. Almulaiky, M. Bilal, Covalent organic frameworks as emerging host platforms for enzyme immobilization and robust biocatalysis – A review, Int. J. Biol. Macromol. 167 (2021) 502–515, https://doi.org/10.1016/j.ijbiomac.2020.12.002.
[8] F.L. Oliveira, A. de S. França, A.M. de Castro, R.O.M. Alves de Souza, P.M. Esteves, R.S.B. Gonçalves, Enzyme Immobilization in Covalent Organic Frameworks: Strategies and Applications in Biocatalysis, Chempluschem 85 (2020) 2051–2066. https://doi.org/10.1002/cplu.202000549.
[9] L. Guo, L. Yang, M. Li, L. Kuang, Y. Song, L. Wang, Covalent organic frameworks for fluorescent sensing: Recent developments and future challenges, Coord. Chem. Rev. 440 (2021) 213957, https://doi.org/10.1016/j.ccr.2021.213957.
[10] R. Xue, Y.-S. Liu, S.-L. Huang, G.-Y. Yang, Recent Progress of Covalent Organic Frameworks Applied in Electrochemical Sensors, ACS Sens 8 (2023) 2124–2148, https://doi.org/10.1021/acssensors.3c00269.
[11] J.M.C. Cifuentes, F.J.F.S. Henrique, C.B.P. Ligiéro, P.M. Esteves, C.D. Buarque, Covalent Organic Frameworks as a Versatile Platform for Iron-Catalyzed sp ^{3} C–H Activation and Cross-Coupling via Decarboxylative Oxidation, Eur. J. Inorg. Chem. (2024), https://doi.org/10.1002/ejic.202300762.
[12] J. Guo, D. Jiang, Covalent organic frameworks for heterogeneous catalysis: principle, current status, and challenges, ACS Cent. Sci. 6 (2020) 869–879, https://doi.org/10.1021/acscentsci.0c00463.
[13] H. Li, A. Dilipkumar, S. Abubakar, D. Zhao, Covalent organic frameworks for CO $_2$ capture: from laboratory curiosity to industry implementation, Chem. Soc. Rev. 52 (2023) 6294–6329, https://doi.org/10.1039/D2CS00465H.
[14] S.S. Han, H. Furukawa, O.M. Yaghi, W.A. Goddard, Covalent Organic Frameworks as Exceptional Hydrogen Storage Materials, J. Am. Chem. Soc. 130 (2008) 11580–11581, https://doi.org/10.1021/ja803247y.
[15] J. Wang, S. Zhuang, Covalent organic frameworks (COFs) for environmental applications, Coord. Chem. Rev. 400 (2019) 213046, https://doi.org/10.1016/j.ccr.2019.213046.
[16] G. Li, B. Yuan, S. Chen, L. Gan, C. Xu, Covalent Organic Frameworks-TpPa-1 as an Emerging Platform for Electrochemical Sensing, Nanomaterials 12 (2022) 2953, https://doi.org/10.3390/nano12172953.
[17] Y. Cao, R. Wu, Y.-Y. Gao, Y. Zhou, J.-J. Zhu, Advances of Electrochemical and Electrochemiluminescent Sensors Based on Covalent Organic Frameworks, Nanomicro Lett 16 (2024) 37, https://doi.org/10.1007/s40820-023-01249-5.
[18] Y.-H. Pang, Y.-Y. Huang, L. Wang, X.-F. Shen, Y.-Y. Wang, Determination of bisphenol A and bisphenol S by a covalent organic framework electrochemical sensor, Environ. Pollut. 263 (2020) 114616, https://doi.org/10.1016/j.envpol.2020.114616.
[19] Z. Lu, Z. Shi, S. Huang, R. Zhang, G. Li, Y. Hu, Covalent organic framework derived Fe3O4 / N co-doped hollow carbon nanospheres modified electrode for simultaneous determination of biomolecules in human serum, Talanta 214 (2020) 120864, https://doi.org/10.1016/j.talanta.2020.120864.
[20] F.-Z. Cui, J.-J. Xie, S.-Y. Jiang, S.-X. Gan, D.-L. Ma, R.-R. Liang, G.-F. Jiang, X. Zhao, A gaseous hydrogen chloride chemosensor based on a 2D covalent organic framework, Chem. Commun. 55 (2019) 4550–4553, https://doi.org/10.1039/C9CC01548E.
[21] T. Zhang, S. Huang, M. Wang, N. Yang, H. Zhu, Integrated untargeted and targeted proteomics to unveil plasma prognostic markers for patients with acute paraquat poisoning: A pilot study, Food Chem. Toxicol. 182 (2023) 114187, https://doi.org/10.1016/j.fct.2023.114187.
[22] E.W. Wang, M.L. Trojano, M.M. Lewis, G. Du, H. Chen, G.L. Brown, L.C. Jellen, I. Song, E. Neely, L. Kong, J.R. Connor, X. Huang, *HFE* H63D Limits Nigral Vulnerability to Paraquat in Agricultural Workers, Toxicol. Sci. 181 (2021) 47–57, https://doi.org/10.1093/toxsci/kfab020.
[23] M. Sharma, N. Maheshwari, F.H. Khan, R. Mahmood, Carbendazim toxicity in different cell lines and mammalian tissues, J. Biochem. Mol. Toxicol. 36 (2022), https://doi.org/10.1002/jbt.23194.
[24] T. Zhou, T. Guo, Y. Wang, A. Wang, M. Zhang, Carbendazim: Ecological risks, toxicities, degradation pathways and potential risks to human health, Chemosphere 314 (2023) 137723, https://doi.org/10.1016/j.chemosphere.2022.137723.
[25] R.A. Maia, F.L. Oliveira, M. Nazarkovsky, P.M. Esteves, Crystal Engineering of Covalent Organic Frameworks Based on Hydrazine and Hydroxy-1,3,5-Triformylbenzenes, Cryst. Growth Des. 18 (2018) 5682–5689, https://doi.org/10.1021/acs.cgd.8b01110.
[26] N. Sarigul, F. Korkmaz, İ. Kurultak, A New Artificial Urine Protocol to Better Imitate Human Urine, Sci. Rep. 9 (2019) 20159, https://doi.org/10.1038/s41598-019-56693-4.
[27] T.S. Martins, J.L. Bott-Neto, O.N. Oliveira Jr, S.A.S.S. Machado, O.N. Oliveira, S.A. S.S. Machado, Paper-based electrochemical sensors with reduced graphene nanoribbons for simultaneous detection of sulfamethoxazole and trimethoprim in water samples, J. Electroanal. Chem. 882 (2021) 114985, https://doi.org/10.1016/j.jelechem.2021.114985.
[28] T.S. Martins, S.A.S. Machado, O.N. Oliveira, J.L. Bott-Neto, Optimized paper-based electrochemical sensors treated in acidic media to detect carbendazim on the skin of apple and cabbage, Food Chem. 410 (2023) 135429, https://doi.org/10.1016/j.foodchem.2023.135429.
[29] A. Barbosa de Sousa, P. Rohr, H.C.S. Silveira, Analysis of mitochondrial DNA copy number variation in Brazilian farmers occupationally exposed to pesticides, Int. J. Environ. Health Res. (2023) 1–10, https://doi.org/10.1080/09603123.2023.2280147.
[30] A.C. Neuber, C.H. Tostes, A.G. Ribeiro, G.T. Marczynski, T.T. Komoto, C.D. Rogeri, V.D. da Silva, E.C. Mauad, R.M. Reis, M.M.C. Marques, The biobank of barretos cancer hospital: 14 years of experience in cancer research, Cell Tissue Bank. 23 (2022) 271–284, https://doi.org/10.1007/s10561-021-09941-9.
[31] Y. Liu, X. Yan, Y. Xing, P. Zhao, Y. Zhu, L. Li, N. Liu, Z. Zhang, Dispersed Au Nanoparticles Anchored on Covalent Organic Frameworks/Carbon Nanotubes via Self-Reduction for Electrochemical Sensing of Acetaminophen, ACS Appl Nano Mater 7 (2024) 4980–4988, https://doi.org/10.1021/acsanm.3c05742.
[32] H.V. Babu, M.G.M. Bai, M. Rajeswara Rao, Functional π-Conjugated Two-Dimensional Covalent Organic Frameworks, ACS Appl. Mater. Interfaces 11 (2019) 11029–11060, https://doi.org/10.1021/acsami.8b19087.
[33] W. Li, T. Xie, X. Chen, J. Lu, R. Qiu, J. Chu, R. Lin, G. Xie, D. Wu, N-doped reduced graphene oxide supported Pd-doped lanthanum vanadate constructs an electrochemical sensing platform for simultaneous detection of carbendazim and methyl parathion in food, J. Food Compos. Anal. 124 (2023) 105647, https://doi.org/10.1016/j.jfca.2023.105647.
[34] T. Kokulnathan, T.-J. Wang, F. Ahmed, N. Arshi, Fabrication of flower-like nickel cobalt-layered double hydroxide for electrochemical detection of carbendazim, Surf. Interfaces 36 (2023) 102570, https://doi.org/10.1016/j.surfin.2022.102570.
[35] W. Li, P. Wang, B. Chu, X. Chen, Z. Peng, J. Chu, R. Lin, Q. Gu, J. Lu, D. Wu, A highly-sensitive sensor based on carbon nanohorns@reduced graphene oxide coated by gold platinum core–shell nanoparticles for electrochemical detection of carbendazim in fruit and vegetable juice, Food Chem. 402 (2023) 134197, https://doi.org/10.1016/j.foodchem.2022.134197.
[36] A. Krishnapandi, S.M. Babulal, S.-M. Chen, S. Palanisamy, S.-C. Kim, M. Chiesa, Surface etched carbon nanofiber companied ytterbium oxide for pinch level

detection of fungicides carbendazim, J. Environ. Chem. Eng. 11 (2023) 109059, https://doi.org/10.1016/j.jece.2022.109059.
[37] L.R. Guterres Silva, J. Santos Stefano, R. Cornélio Ferreira Nocelli, Campos Janegitz, 3D electrochemical device obtained by additive manufacturing for sequential determination of paraquat and carbendazim in food samples, Food Chem. 406 (2023) 135038, https://doi.org/10.1016/j.foodchem.2022.135038.
[38] R. Zhou, L.-Z. Liu, Y.-H. Pang, X.-F. Shen, Cerium metal-organic framework composited with polyaniline on carbon cloth for high-sensitively electrochemical sensing of carbendazim, Microchem. J. 197 (2024) 109862, https://doi.org/10.1016/j.microc.2023.109862.
[39] D.M. Sajjan, D. Ilager, M.M. Shanbhag, M.A. Alshehri, N.P. Shetti, Rapid and facile electrochemical detection and degradation of carbendazim in the spiked environmental trials using reduced graphene oxide/titanium dioxide-based sensor, J. Environ. Chem. Eng. 12 (2024) 112946, https://doi.org/10.1016/j.jece.2024.112946.
[40] E. Hou, Z. Kong, J. Wu, H. Wang, P. Nie, M. Lu, L. Chang, Preparation of Ag–TiO2/MXene composite material for electrochemical detection of paraquat, J. Mater. Sci. Mater. Electron. 34 (2023) 1177, https://doi.org/10.1007/s10854-023-10603-7.
[41] S.C. Teixeira, N.O. Gomes, M.L. Calegaro, S.A.S. Machado, T.V. de Oliveira, N. de Fátima Ferreira, P.-P. Soares, Sustainable plant-wearable sensors for on-site, rapid decentralized detection of pesticides toward precision agriculture and food safety, Biomaterials Advances 155 (2023) 213676, https://doi.org/10.1016/j.bioadv.2023.213676.
[42] S. Sain, M. Ficek, A. Olejnik, M. Sawczak, R. Bogdanowicz, S.S. Roy, Direct determination of paraquat herbicide by square-wave voltammetry by two-step transfer mechanism at heterogeneous boron-doped carbon nanowall electrodes, Diam. Relat. Mater. 140 (2023) 110504, https://doi.org/10.1016/j.diamond.2023.110504.
[43] D. Moodley, X. Nocanda, P. Nelson, A. Mambanda, I.N. Booysen, Construction of a Functional and Robust Cobalt(II) Phthalocyanine-Modified Electrode for the Electrocatalytic Detection of Paraquat, ChemElectroChem (2023), https://doi.org/10.1002/celc.202300427.
[44] W. Thongsomboon, J. Sonjai, J. Jakmunee, J. Lerdsri, P. Reanpang, J. Upan, Manganese oxide@nanocellulose modified poster paper-based electrode as a novel electrochemical sensor for sensitive determination of paraquat, J. Appl. Electrochem. (2023), https://doi.org/10.1007/s10800-023-02023-6.
[45] C. Yuan, C. Tang, X. Zhan, M. Zhou, L. Zhang, W.-T. Chen, A. Abdukayum, G. Hu, ZIF-67 based CoS2 self-assembled on graphitic carbon nitride microtubular for sensitive electrochemical detection of paraquat in fruits, J. Hazard. Mater. 467 (2024) 133715, https://doi.org/10.1016/j.jhazmat.2024.133715.
[46] D. Pimalai, T. Putnin, S. Bamrungsap, A highly sensitive electrochemical sensor based on poly(3-aminobenzoic acid)/graphene oxide-gold nanoparticles modified screen printed carbon electrode for paraquat detection, J. Environ. Sci. 148 (2025) 139–150, https://doi.org/10.1016/j.jes.2023.10.006.
[47] G.K. Ramos, D.S. Goldfarb, Update on Uric Acid and the Kidney, Curr. Rheumatol. Rep. 24 (2022) 132–138, https://doi.org/10.1007/s11926-022-01069-3.
[48] L.M. Peña-Acevedo, D.A. Ballesteros-Castro, C.A. Sukumar, Paraquat, in: Encyclopedia of Toxicology, Elsevier, 2024: pp. 269–281. https://doi.org/10.1016/B978-0-12-824315-2.00666-7.